IEEE Access
Multidisciplinary | Rapid Review | Open Access Journal

Received November 7, 2019, accepted November 29, 2019, date of publication December 4, 2019,
date of current version December 17, 2019.

Digital Object Identifier 10.1109/ACCESS.2019.2957515

Transverse Damage Localization and Quantitative Size Estimation for Composite Laminates Based on Lamb Waves

M. SAQIB HAMEED AND ZHENG LI
State Key Laboratory for Turbulence and Complex Systems, Department of Mechanics and Engineering Science, College of Engineering, Peking University, Beijing 100871, China

Corresponding author: Zheng Li (lizheng@pku.edu.cn)

This work was supported by the National Natural Science Foundation of China under Grant 11521202.

ABSTRACT The damage detection method for composite laminates introduced in this research uses piezoelectric (lead zirconate titanate, PZT) transducers to excite/sense the Lamb wave signals. The complicated wave signals scattered by damage are accurately processed using a continuous wavelet transformation (CWT) based on the Gabor wavelet. The transducers are arranged on a composite laminate in the form of a network of square detection cells and triangular subcells. The damage location is estimated using the concept of centroid in two-stage detection method. The first stage detection is carried out by exciting a transducer at the center of each detection cell to locate the damaged cell and subcell. The damage localization is improved by exciting an additional transducer at the corner of the damaged subcell during the second stage detection. The damage size is then quantitatively estimated using cubic spline curve (CSC) and elliptical parametric (EP) methods based on the damage edge points. The damage location is estimated in two detection stages for high-accuracy because the damage edge points are calculated with reference to the estimated location of the damage. The arrangement of transducers and signal processing technique remain the same at all the stages of damage detection. Results from previous detection stages contribute to the improvement of damage detection in the subsequent stages. The size of detection cell plays a crucial role in designing the detection stages, and the proposed method can accurately quantify both location and size of the damage in composite laminate.

INDEX TERMS Composite laminate, PZT transducer, continuous wavelet transform, damage size quantification, elliptical reconstruction.

I. INTRODUCTION

The properties of composite materials can be tailored to exhibit superior properties such as high strength to weight ratio, high modulus and high resistance to aggressive environmental conditions. Composite materials are increasingly employed to achieve the desired performance in wide range of applications from various industries like aerospace, automotive, naval and wind turbine etc. However, the mechanical properties and structural integrity of composite structures can be compromised by various types of fabrication and in-service defects. A small damage in composite structure can grow and lead to the catastrophic failure of the entire structure. Therefore, a continuous monitoring of the structural components, for damage detection at an early stage, is required for efficient repair and maintenance. Researchers have developed many computational and intelligent techniques for structural health monitoring (SHM) of composites [1]. The SHM techniques based on Lamb waves are commonly used for damage detection in composite laminates. The Lamb waves are highly sensitive to small imperfections, and have the ability to propagate relatively a long distance with low attenuation. The change in the Lamb wave propagation due to forward and backward scattering from damage can be analyzed to evaluate the damage. The PZT (lead zirconate titanate) transducers are frequently used to excite and sense the Lamb wave signals because they are small, lightweight, consume low power, and produce a frequency response in wide region [2]. For fast and in situ SHM, PZT transducers can be directly

The associate editor coordinating the review of this manuscript and approving it for publication was Yingxiang Liu.

attached to the surface of host structure in the form of a network of sensors to record multipoint measurements. However, sophisticated signal-processing techniques are required to physically interpret the dispersive and multi-modal Lamb wave signals scattered by damage. The time of flight (ToF) based damage detection methods are frequently used for composite laminates. A variety of techniques for an accurate ToF measurement have been developed including, continuous wavelet transform (CWT) [2], [3], short-time Fourier transform (STFT) [5], warped frequency transform (WFT) [6] and matching pursuit (MP) algorithm [7]. Furthermore, the accurate ToF measurement has been utilized for the elliptical reconstruction of the damage, and various imaging algorithms have been developed for damage localization like non-contact type laser excitation sparse imaging [8], minimum variance distortionless response (MVDR) method [9], iterative algebraic reconstruction technique (ART) [10], reconstruction algorithm for probabilistic inspection of damage (RAPID) [11], probability-based diagnostic imaging (PDI) [12] and least-squares reverse time migration (LSRTM) [13].

The concept of the Lamb wave signals reflecting from the damage boundary has been used to find the reflection points on damage. These reflection points have been then used to reconstruct the damage images for plate-like structures. A damage size characterization algorithm was developed for estimation of corrosion in aluminum plates [14]. The wave scattering source was estimated as one point on damage boundary for each sensing path. The convex hull was then applied to these points on damage boundary to approximate the shape and size of the damage. The concept of reflection points on damage boundary was used to develop two different active sensing methods, a damage index method and a diagnostic imaging method, for damage detection in isotropic and composite structures [15]. The reflection points were determined as special point on each elliptical path loci with the shortest distance to the center of curvature of damage boundary [16]. The convex envelope was then identified by using the reflection points to represent the damage shape. However, the location of damage was supposed to be already known in order to estimate its size. The reflection points were defined as front points on damage for developing a theory to evaluate the reflection intensity of Lamb waves [17]. This theory could quantify the size of circle-like damage in aluminum plate with unneglectable errors. A method based on finding the damage contour using convex envelope of damage reflection points has been presented where, the delamination was modeled in composite laminates [18]. The evaluation of damage shape and size by determining the wave scattering sources for different sensing paths was utilized for the development of enhanced ellipse and probabilistic imaging algorithms for composite laminates [19]. Damage detection based on Lamb wave focusing by an array of PZT transducers has improved the detection resolution using dispersion compensation. The resolution of the method depends on the number of focusing points on the structure under inspection [20]. A method based on the compressed sensing was introduced to address the dispersion compensation for both single and multi-mode guided wave problems. A dispersion signal dictionary was built by using the dispersion curves of guided wave modes. The dispersion-compensated waves were then obtained by utilizing a non-dispersion signal dictionary and the results of sparse decomposition [21]. A two-stage damage estimation method was introduced to identify the location and size of the multiple damage inside the individual layers of the laminated composite beams [22]. The damage was localized in the first stage by using the normalized cumulative energy, and then extent of the damage was measured in the second stage by solving an optimization problem via differential evolution algorithm. An efficient approach for optimal sensor placement (OSP) using iterated improved reduced system (IIRS) method was proposed and applied to the damage identification in composite laminates [23]. Bayes' theorem updated the probability distributions of the parameters by combining the prior information and measured ToF data for damage localization in composite laminates [4]. In order to improve the imaging capability for damage localization in complex structures, the defect distribution probability of PDI algorithm was modified to develop an elliptical ring distribution probability-based diagnostic imaging algorithm [24]. Two ToF based damage localization methods were proposed for composite laminates [25]: the first algorithm used the probabilistic approach by constructing a probability matrix for locating the defects with large errors, and the second algorithm based on the artificial neural networks was then used to improve the accuracy of defect localization. The near-field sampling phased-array damage monitoring algorithm was combined with the two-dimensional phased-array in an omnidirectional damage imaging method [26].

In the aforementioned methods, the researchers mostly simulated the defects using circular [3], [9], [10], [13], [14], [18]–[20], [22]–[24], square [12], [25] and rectangular [15], [17] shapes, which may not be the best representation of the actual damage in composite laminates. Studies performed at the microscopic level reveal that the more realistic representation of damage is the thin and elongated ellipse-like shape [31], which has been used to simulate the damage in composite laminates [27]–[30]. In addition to that, the methods discussed here have used a large number of PZT transducers just to locate the damage of simplistic shapes. For example, the methods for locating the circular damage have used 16 transducers with 56 pitch-catch signal acquisition paths [14], 30 distributed transducers [15], 16 transducers with 28 sensing paths [24] and 12 transducers with 84 sensing paths [11]. The use of too many PZT transducers requires a big amount of data to be processed during the SHM process. Therefore, there is a need to develop fast and in situ SHM methods for on-line monitoring of composite structures with minimum data recording. Furthermore, most of the existing elliptical reconstruction methods are image-based which focus only on damage localization [3], [9], [10], [12]–[14], [18]–[22], [24], [25], [31],

and do not provide the quantitative estimation of damage size/extent.

In this research, the PZT transducers were arranged in the form of a network of square detection cells on a CFRP composite laminate. Each cell was comprised of just 5 transducers: 1 at center and 4 at the corners of the cell. The damage location was first estimated accurately in two stages using the centroid of intersections of elliptical path loci, which was then used to calculate the damage edge points. The damage size was quantitatively estimated using the Cubic Spline Curve (CSC) and Elliptical Parametric (EP) methods which were based on damage edge points. The CSC method fitted a spline curve through the damage edge points instead of the widely used convex hull/envelope whereas, the EP method estimated the parameters of the damage in order to reconstruct the damage as an ellipse. It is found that the EP method can quantify the size of the elliptical damage with more accuracy than the CSC method. The method requires a relatively smaller amount of data to be collected, and it is more accurate compared to the existing ellipse-based reconstruction methods for damage size quantification.

The organization of this article is as follows: Section II introduces the theory of the proposed damage detection methods. The dispersion curves are presented in Section III. The finite element (FE) model and its validation is presented in Section IV. The damage detection strategy and its implementation are shown in Section V. The procedure for damage localization in two stages is presented in Section VI. Section VII includes the damage size estimation using CSC and EP methods. The influence of noise on the accuracy of the method is studied in section VIII. The article is then summed up with a discussion of results in Section IX, and conclusion in Section X.

II. DAMAGE DETECTION METHODOLOGY

Consider a unit cell from the network of PZT transducers in a plate structure with four transducers (P1-P4) arranged in square configuration, and a circular damage located at P5(x, y) from the center of the cell, as shown in Figure 1. One of the transducers, for example P1, acts as an actuator to induce the Lamb waves that propagate radially outward. The other three transducers (P2-P4) act as sensors to receive the direct signal from P1, and also the signal scattered by the damage. The direct signal from P1 propagates a distance d and arrives at P4 with a ToF t_{14}. However, there is an additional signal received at P4 which is scattered by the damage, and travels a longer distance $d_1 + d_2$ with a longer ToF $t_{15} + t_{54}$. The difference between the ToF of direct and damage-scattered signals is delay time Δt_{14}, calculated from

$$(d_1 + d_2) - d = v \times \left[(t_{15} + t_{45}) - t_{14}\right] = v \cdot \Delta t_{14} \quad (1)$$

where, v is the group velocity. The distance d is known as the distance between prearranged transducers whereas, the distances d_1 and d_2 can be calculated using the geometric relations in Figure 1. Therefore, the Equation (1) can be

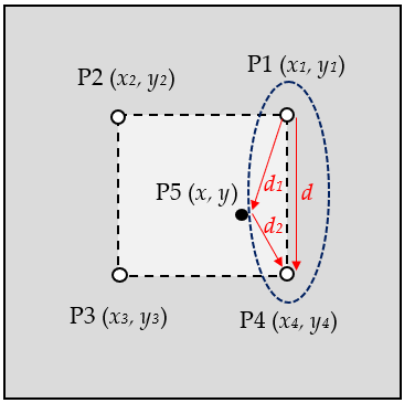

FIGURE 1. The PZT transducers arranged on a damaged plate with an ellipse tangent to the damage.

rewritten as,

$$\sqrt{(x_1 - x)^2 + (y_1 - y)^2} + \sqrt{(x_4 - x)^2 + (y_4 - y)^2} = v \cdot \Delta t_{14} + d \quad (2)$$

For a known value of Δt_{14}, Equation (2) represents an ellipse with focal points at P1 and P4, as shown with the blue dashed line in Figure 1. Similarly, if the delay times between P1-P2, P2-P3 and P3-P4 are known, a total of four ellipses can be drawn with one ellipse along each side of the square cell formed by the transducers, as shown in Figure 2(a). The ellipses obtained from different actuator-sensor combinations will not perfectly intersect at a single point as the damage has non-ignorable size, and it cannot be considered as a point [25]. Consequently, the Lamb wave signals reflect from the outer periphery of the damage, and the ellipses remain externally tangent to the damage boundary [32]–[34], as shown in Figure 2(b). It can be further seen in Figure 2(b) that due to the significant damage size, the intersection of elliptical path loci deviates from the actual damage location. Therefore, the performance of the traditional ellipse-based methods introduced in section I may be restricted.

A. DAMAGE LOCALIZATION

The concept of centroid based on the intersections of path loci is adopted for the localization of damage with non-ignorable size. The centroid represents the location (x, y) of the damage, and it can be calculated using the statistical intersection results of the elliptical path loci and defined as,

$$(x, y) = \sum_{i=1}^{n} \frac{(x_i, y_i)}{n}$$

where, (x_i, y_i) are the coordinates of the ith intersection point, and n is the total number of intersection points. All the intersection points of the path loci are encircled with red marker in Figure 2(b). The centroid, represented with red cross in Figure 2(b), is calculated using every neighboring path locus intersection which minimizes the measurement error induced in an individual intersection value. There can be

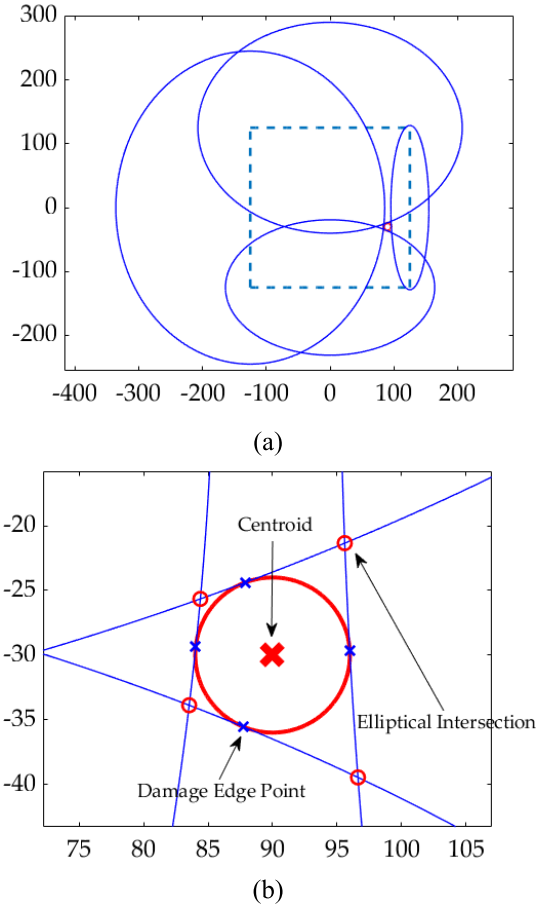

FIGURE 2. (a) Four elliptical path loci surrounding a circular damage. (b) Representation of centroid and edge points on damage using the intersections of externally tangent path loci.

single or double intersections between each pair of elliptical path loci, and it is also possible that there is no intersection. For the case when there are two intersections for one pair, one of the intersection points lying far from damage will be unwanted, as it will have limited influence on centroid estimation. For example, it can be observed in Figure 2(a) that there are many intersections which happen to be outside the square monitoring region represented by dashed line, these intersections can be ignored for centroid calculation.

B. DAMAGE SIZE QUANTIFICATION

Since, the wave signals are reflected from the outer periphery of the damage, therefore, each path loci will intersect the damage boundary only at one point. When location of the damage is known, this point is one of the points on elliptical path loci which has the minimum distance from the damage center (x, y) as,

$$(x_e, y_e) = \min_{(x,y)} \sqrt{(x_k - x)^2 + (y_k - y)^2} \tag{3}$$

where, (x_k, y_k) are all the points on the elliptical path loci. This point (x_e, y_e) is called the damage edge point in this research, and all the damage edge points are represented with

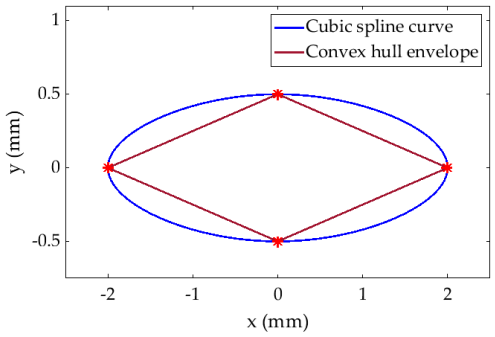

FIGURE 3. An example of damage contour estimation using damage edge points.

blue cross in Figure 2(b). The distribution of damage edge points is useful to construct the damage shape and estimate its size quantitatively. In the following subsections, two different methods for damage size estimation are introduced based on the known values of damage edge points.

1) CUBIC SPLINE CURVE (CSC) METHOD

Periodic interpolating cubic spline curve generates a parametric variational curve passing through the given sequence of points. The parameter value for any point is chosen by Eugene Lee's centripetal scheme [39], which is the accumulated square root of the chord length. To construct a periodic cubic spline curve, the first and the last points should coincide, and there should be no repeated points. In CSC method, a *MATLAB* tool package named *cscvn* is utilized to construct the cubic spline curve passing through all the damage edge points. An example cubic spline curve drawn using *cscvn* which passed through a given set of 4 damage edge points is presented in Figure 3. The cubic spline curve is compared with the widely used convex hull envelope passing through the same set of edge points in Figure 3. It can be observed that the cubic spline curve constructs the elliptical damage with more accuracy than the convex hull envelope, especially when there are a few damage edge points available. The resultant curve in CSC method represents the approximate contour of the reconstructed damage, and the area enclosed by this curve quantifies its size.

2) ELLIPTICAL PARAMETRIC (EP) METHOD

There are existing methods for composite laminates which can accurately estimate the size of circular damage but cannot quantify a narrow and long damage like transverse or fatigue cracking. The Lamb waves are highly sensitive to transverse defects like delamination and debonding in composite laminates [40]. When a point or circular damage expands in size, it becomes thin and elongated, and its shape adopts an ellipse-like contour. Although, the Lamb wave signals still reflect from the out periphery of an elliptical damage but the path loci do not intersect the damage boundary only at one point like in the case of a circular damage shown in Figure 2(b). It is because the ellipse does not have a fixed radius like a circle, so the path loci intersect the damage

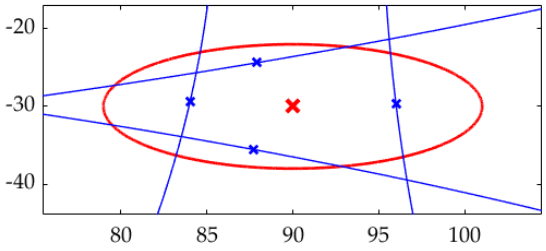

FIGURE 4. Interaction of path loci with an elliptical damage.

boundary in way that a part of it falls inside the damage region, and does not remain exactly tangent to the damage boundary, as shown in Figure 4. Therefore, the maximum and minimum distances between any two damage edge points will always be shorter than the length of the major and minor axis, respectively, of the elliptical damage.

The EP method is based on estimating these defects with an ellipse whose parameters are calculated using the damage edge points. The maximum distance between any two damage edge points represents the length of semi-major axis, a, while, the minimum distance between any two edge points represents the length of semi-minor axis, b, of an ellipse, as follows

$$a = \max \frac{\sqrt{\left(x_{e_i} - x_{e_j}\right)^2 + \left(y_{e_i} - y_{e_j}\right)^2}}{2}$$

$$b = \min \frac{\sqrt{\left(x_{e_i} - x_{e_j}\right)^2 + \left(y_{e_i} - y_{e_j}\right)^2}}{2}$$

where, $(i, j) = 1, ..., n, i \neq j$, and n is total number of damage edge points. The size of the damage (A_d) can be then calculated by finding the area of ellipse formed by a and b as,

$$A_d = \pi ab$$

The circular damage is a special case in EP method when the lengths a and b are equal to radius r, and the size of damage can be calculated using the area of a circle as, πr^2.

III. DISPERSION CURVES

An infinite number of guided wave modes can be excited in a thin plate with two surfaces. The group velocity of Lamb waves varies as the product of signal frequency and thickness of the plate varies. The dispersion curves for Lamb waves in CFRP composite laminate along 0° direction with respect to the fiber orientation in quasi-isotropic layup $[0/90/+45/-45]_S$ were drawn using the reverberation-ray matrix method [41], presented in Figure 5. The dispersive and multimode characteristics of Lamb waves can be observed in the dispersion curves at low frequency range with both symmetric (S_0) and asymmetric (A_0) modes propagating simultaneously.

The two fundamental modes of Lamb wave (S_0, A_0) propagate simultaneously at a low-frequency range in Figure 5. However, the S_0 mode has much higher group velocity than the A_0 mode. If a modified signal with a narrow frequency

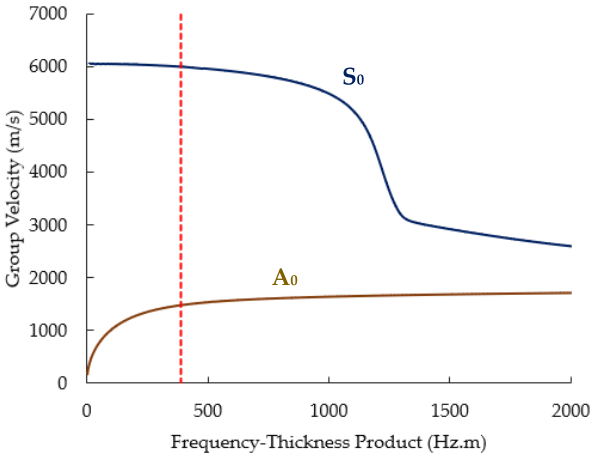

FIGURE 5. Group velocity dispersion curves of $[0/90/+45/-45]_S$ composite laminate along 0° direction.

TABLE 1. Elastic constants of a single lamina.

ρ (kg m^{-3})	E_1 (GPa)	E_2 (GPa)	G_{12} (GPa)	ν_{12}	ν_{23}
1520.7	127.70	9.6677	6.4955	0.3001	0.3292

band is used, both the modes can be identified separately with the peak of S_0 mode arriving first, and the A_0 mode arriving later. In the mode conversion after scattering from the damage, the S_0 reflects a faster symmetric mode S_0, and a slower antisymmetric mode A_0 [42]. The S_0 mode is preferred for damage detection in majority of research due to its fast propagation velocity and easy identification as compared to the A_0 mode. Furthermore, in different composite layups and along all other propagation directions, the dispersion curves of Lamb waves have the similar property [1], [38]. Therefore, the scattered S_0 mode as the one propagating faster [39], [40], was exclusively considered for the proposed method.

IV. FE SIMULATION MODEL

The numerical simulations were conducted on $1000 \times 1000 \times 1.5$ mm^3 CFRP composite laminate using a commercial FE software ABAQUS explicit. The layup $[0/90/+45/-45]_S$ was used with thickness of a single lamina as 0.1875 mm, and the elastic constants listed in Table 1.

The diameter of each PZT transducer was 8 mm, and it could excite and sense the Lamb wave signals in radially outward directions. The FE mesh should have at least 8-10 nodes per Lamb wavelength for accurate characterization of Lamb wave signals propagating in a damaged plate [46]. The plate was meshed with 3D shell element S4R which uses six degrees of freedom at all nodes. The element size was 0.5 mm which created around 46.5 elements per wavelength for all simulation models. The time step for dynamic calculation must be less than the ratio of minimum distance of any two adjoining nodes to the maximum wave

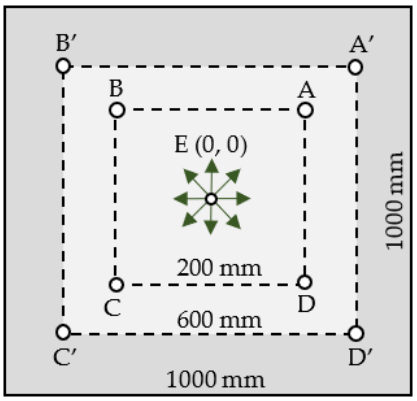

FIGURE 6. PZT transducer configuration to calculate the S_0 mode group velocity.

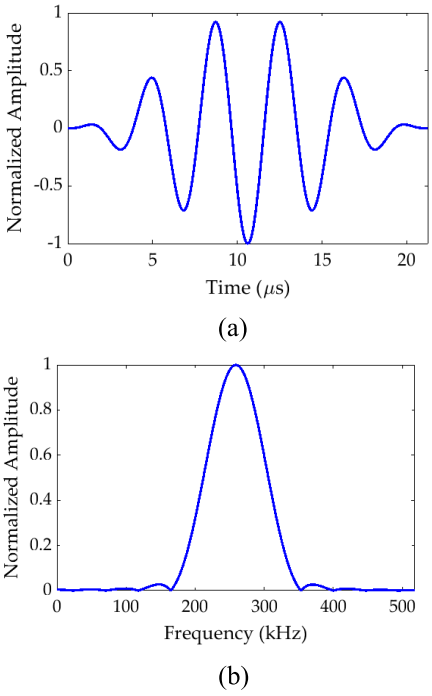

FIGURE 7. The excitation signal: (a) time domain and (b) frequency domain.

velocity [2]. Therefore, for accurately simulating the Lamb wave propagation, a time step of 0.02 μs was given for total time of 150 μs. The simulation model was first validated by calculating the S_0 mode group velocity v by using the transducer configuration shown in Figure 6. The central transducer at point E provided the excitation, and the transducers from A to D and A′ to D′ acquired the response signals.

An in-plane force with a 5.5-cycle sinusoidal tone burst modulated by Hann window at central frequency of 259 kHz, shown in Figure 7, was used as excitation signal. The central transducer E generated the signal, and the frequency (259 kHz) - thickness (1.5 mm) product was 388.5 Hz-m, shown with the red dashed line in Figure 5. This point lay in a low-frequency range, and both S_0 and A_0 wave

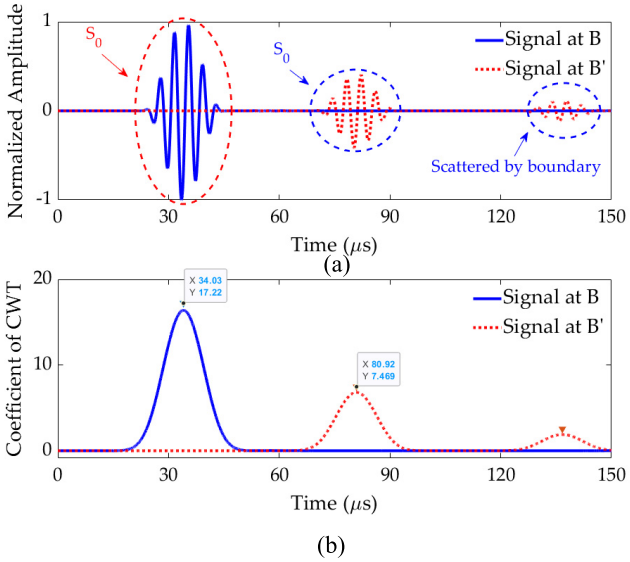

FIGURE 8. (a) Signals received at B and B′. (b) Continuous wavelet transformation (CWT) of signals received at B and B′.

modes existed in the dispersion curves. The S_0 mode was clearly traveling with a higher group velocity than A_0 mode, and could be easily identified at this frequency. The proper wave information was extracted from the complicated signals using CWT based on Gabor wavelet [47], a signal processing technique.

The signals received at A-A′, B-B′, C-C′, and D-D′ were converted to nondimensional form by normalizing with the maximum amplitude. The signals received at B-B′ are plotted in Figure 8(a), and their CWTs are presented in Figure 8(b). The first two arrival peaks were direct excitation signal S_0 at B and B′, received at time $t_1 = 34.03$ μs and $t_2 = 80.92$ μs, respectively, and the third peak was the signal scattered by the plate boundary. Therefore, the traveling time of Lamb waves from B to B′ was the difference between t_1 and t_2, namely, 46.89 μs. The distance between B and B′ was 282.84 mm, and the group velocity was calculated as 6.032×10^3 m/s. The velocity was almost same as that obtained from the dispersion curve in Figure 5 (red dash line; i.e., 6.01×10^3 m/s. The same value of velocity was obtained when calculations were made using the other three set of points; i.e., A-A′, C-C′ and D-D′. This validation proves that the numerical model had good accuracy for simulating the Lamb wave propagation. It further validates that the CWT accurately extracted the ToF/delay time which is important for elliptical reconstruction.

V. DAMAGE DETECTION STRATEGY

The PZT transducers are usually embedded in modern structures during the manufacturing for in situ SHM throughout the service life. The transducers can be arranged as a network of measuring points on large structures like wing of an aircraft or a wind turbine blade. The method introduced in this research proposes a simple network of transducer detection cells, as shown in Figure 9(a). Each square cell is

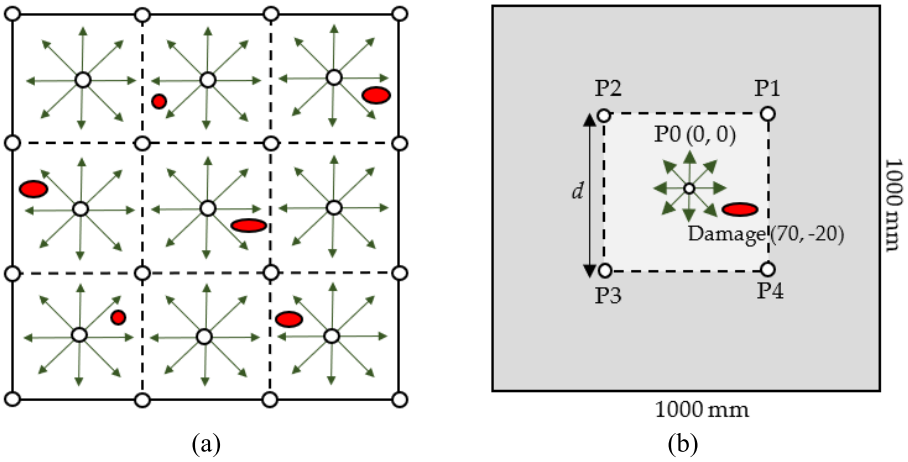

FIGURE 9. (a) Detection cells formed by a network of PZT transducers. (b) A single damaged cell.

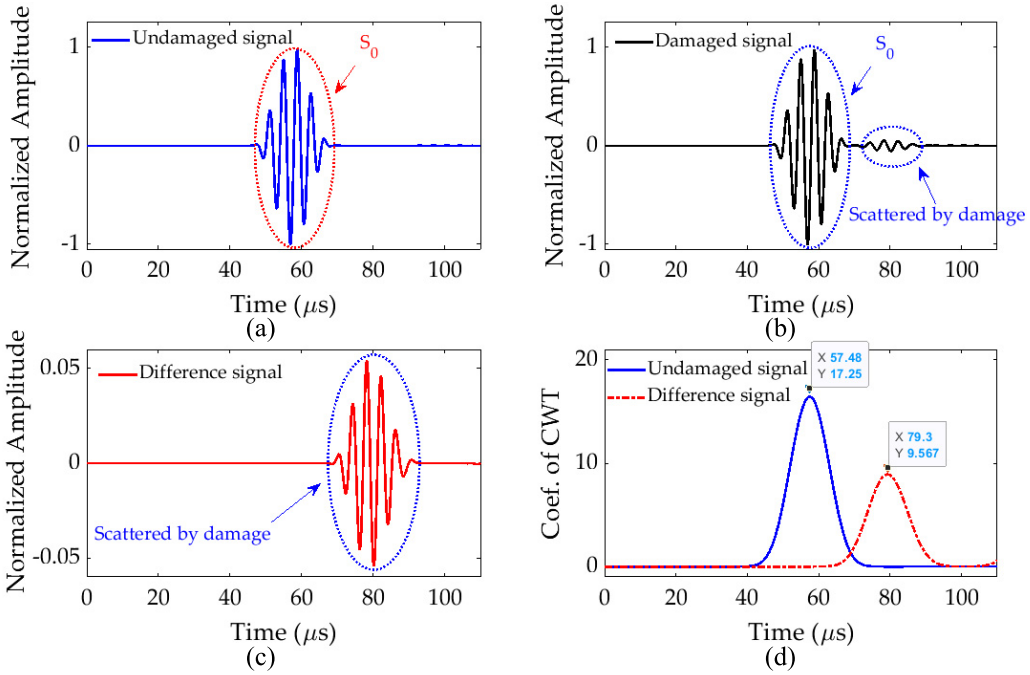

FIGURE 10. Undamaged signal at P2. (b) Damaged signal at P2. (c) Difference between undamaged and damaged signals. (d) CWT of undamaged and difference signals.

comprised of five transducers: four at the corners of the square and one at the center. The single-stage damage detection locates the damaged cell by exciting the central transducer of each square cell separately. Therefore, only a single damaged cell is considered with four PZT transducers located at points P1–P4, as shown in Figure 9(b). The cell under consideration in Figure 9(b) was modelled with an elliptical damage of 10 mm and 4 mm as lengths of the major and minor axis, respectively. The damage was a through-hole with the center of ellipse located at (70, −20) mm, and the distance d between the corner transducers was 400 mm. The direction of elliptical damage is not important at this stage as the transverse cracks are commonly orientated perpendicular to the longitudinal direction.

The central transducer P0 excited the signals, and four corner transducers P1-P4 recorded the dynamic response signals. In order to calculate the delay times for each transducer, the damaged signal was compared with the baseline signal from the undamaged plate. For example, the undamaged signal received at P2 in the intact plate ($d = 400$ mm) is shown in Figure 10(a) which contains the direct excitation signal S_0. The damaged signal at the same point is shown in Figure 10(b), and it contains an additional fluctuation caused by the scattering from damage. The central excita-

TABLE 2. Delay time for transducers at P1–P4 with P0 excitation, $d = 400$ mm.

Delay time (μs)	Δt_{01}	Δt_{02}	Δt_{03}	Δt_{04}
	7.91	21.82	18.36	2.29

tion ensures that the Lamb wave signal first interacts with the damage, and then with the plate boundary. The difference between undamaged and damaged signals (shown in Figure 10(c)) clearly indicates the presence of damage in the plate. The CWTs of undamaged and difference signals are shown in Figure 10(d).

The arrangement of transducers ensured that the Lamb wave signals first interacted with the damage, then propagated towards the nonphysical boundaries of the cell, and further towards the physical boundary of the plate. In order to avoid scattering from the plate boundary, the total time of Lamb wave propagation was kept as 110 μs for this model. Therefore, the delay time for P2 calculated using the difference between the first peaks of undamaged and difference signals is $\Delta t_{02} = 21.82$ μs. Similarly, the delay time $\Delta t_{0i} (i = 1, \ldots, 4)$ could be calculated and is listed in Table 2. The four elliptical path loci, one for each set of actuator-sensor combination, can be drawn using the delay times given in Table 2 for $d = 400$ mm.

VI. DAMAGE LOCATION ESTIMATION

A. SINGLE-STAGE DETECTION

The location of the damage was estimated using the concept of centroid based on the intersections of path loci introduced in section II. In order to study the effect of the cell size on damage localization, the distance d between the corner transducers was varied from 300 mm to 600 mm with the increment of 100 mm, and the path loci were drawn for each value of transducer spacing d.

The path loci for $d = 400$ mm are presented in Figure 11(a), and the six intersections of the path loci are encircled with blue marker in Figure 11(b). Furthermore, the actual damage is shown with a red ellipse, and its location is crossed with red marker. The estimated location using the centroid of elliptical intersections is presented with the blue plus sign marker in Figure 11(b). Similarly, the elliptical path loci and estimated damage location are calculated for different transducer spacing. The estimated damage location in the single-stage damage detection method was (68.01, −19.00) mm, (68.29, −19.13) mm, (68.43, −19.17) mm, and (68.56, −19.24) mm, respectively, for $d = 300, 400, 500, 600$ mm, and the absolute errors were 2.22 mm, 1.92 mm, 1.78 mm, and 1.62 mm, respectively. The results indicate that the damage localization accuracy improves as the size of detection cell increases.

B. TWO-STAGE DETECTION

The single-stage damage detection excited the central transducer at P0, and the four corner transducers acted as receivers. To further analyze the results, the detection cell is divided

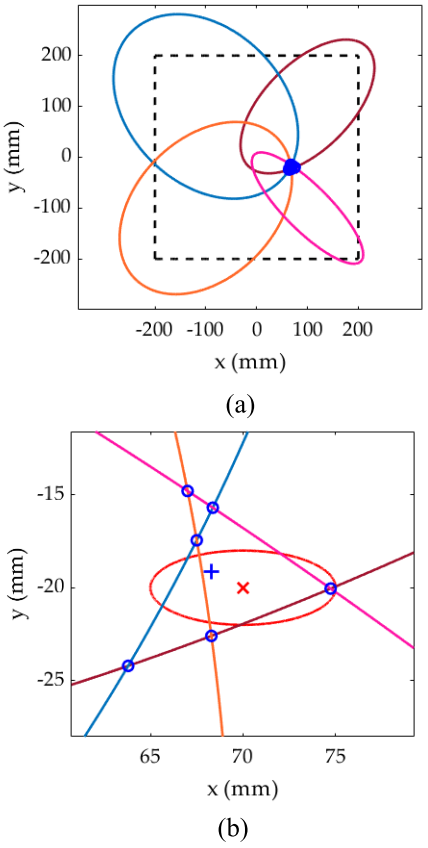

FIGURE 11. (a) Elliptical path loci plotted in single-stage detection. (b) Estimated (blue) and actual (red) damage location. ($d = 400$ mm).

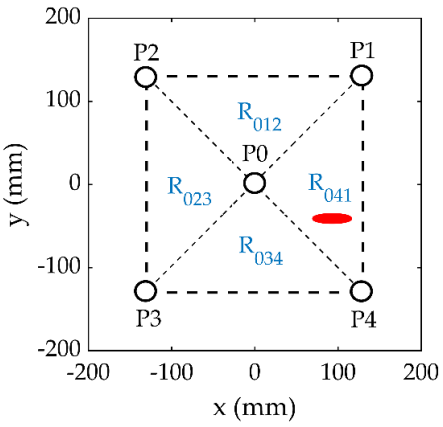

FIGURE 12. Division of a damaged cell into four subcells, and identification of the damaged subcell.

into four triangular subcells with a transducer at each vertex of every triangle. These subcells are represented by R_{ijk} in Figure 12, where the subscripts "ijk" are the identifiers of the three transducers forming the triangular subcell. The damage localization results in single-stage detection were acceptable, and thus could accurately locate the damaged subcell. The single-stage detection results for the simulated case indicate the damage was contained in the subcell R_{041}, as shown in Figure 12. To improve the damage localization the second stage of detection, the damage was

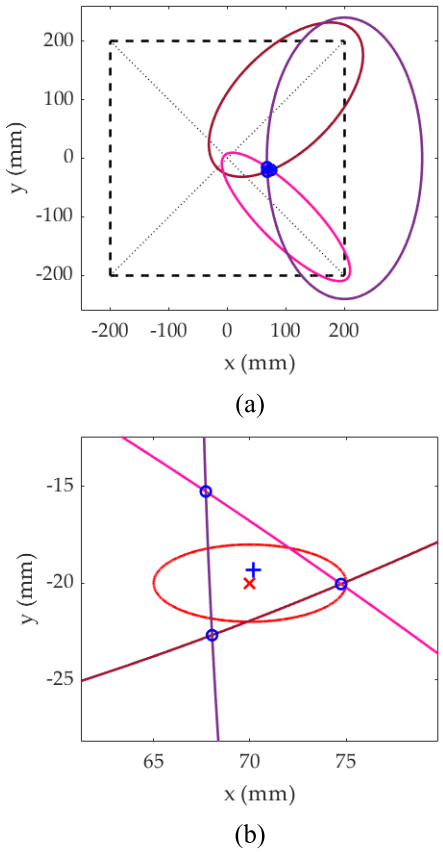

FIGURE 13. (a) Elliptical path loci plotted in two-stage detection. (b) Estimated (blue) and actual (red) damage location. ($d = 400$ mm).

estimated using the three ellipses formed inside the damaged subcell. These ellipses were drawn using the delay times Δt_{01}, Δt_{04}, and Δt_{14} between the points P0–P1, P0–P4, and P1–P4, respectively. The first two ellipses were already formed in the single-stage detection, while an additional third ellipse was formed between the corner transducers P1 and P4 using the delay time Δt_{14}. The delay time Δt_{14} was calculated by exciting any of the corner transducers (P1 or P4), and recording the signal at the other corner transducer. The elliptical path loci and estimated damage location in the second stage detection are presented, respectively, in Figures 13(a) and (b) for d = 400 mm. The damage location estimated through the two-stage detection method was (70.11, −19.14) mm, (70.16, −19.33) mm, (70.56, −19.47) mm, and (70.79, −19.60) mm, respectively, for $d = 300, 400, 500, 600$ mm, and the absolute errors were 0.87 mm, 0.69 mm, 0.77 mm, and 0.89 mm, respectively. The results indicate that damage localization improve using the two-stage damage detection method.

VII. DAMAGE SIZE ESTIMATION

The damage cell and the subcell were located in the single-stage damage detection method, and it was found that the damage localization with bigger transducer spacing is more accurate. Therefore, the damage localization was improved in

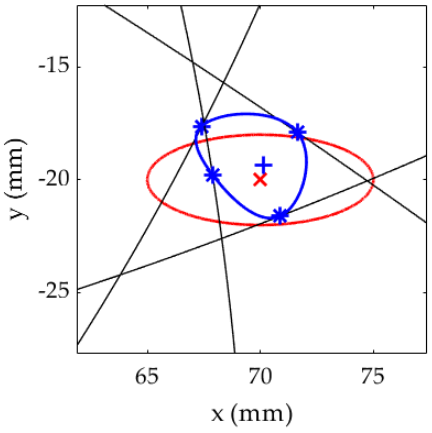

FIGURE 14. Estimated (blue) and actual (red) damage size estimation using CSC method. ($d = 400$ mm).

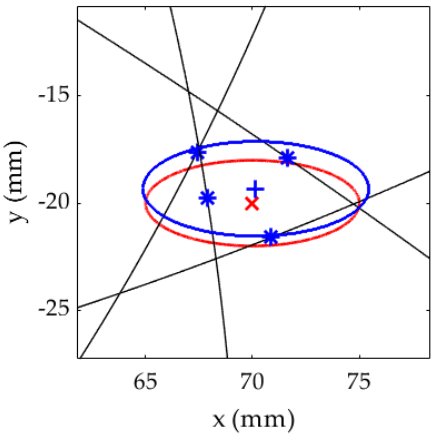

FIGURE 15. Estimated (blue) and actual (red) damage size estimation using EP method. ($d = 400$ mm).

the two-stage damage detection by using an additional ellipse formed between a bigger transducer spacing. The damage edge points were then calculated by finding the minimum distance from the estimated location and any point on the elliptical path loci, as introduced in section II. The additional ellipse formed in the second stage of detection is not needed anymore for size estimation. It was made just to improve the damage localization as the accurate estimation of damage location would ensure the accurate damage edge points. Therefore, the elliptical path loci for single-stage damage detection, already presented in Figure 11, were used for damage edge points and size calculations. The estimated damage along with the damage edge points calculated using the CSC method, introduced in section II, are plotted in Figure 14 for transducer spacing $d = 400$ mm.

The estimated size of the damage was 16.02 mm^2, 16.572 mm^2, 18.592 mm^2, and 16.662 mm^2, respectively, for $d = 300, 400, 500, 600$ mm, and the absolute errors were 15.40 mm^2, 14.84 mm^2, 12.82 mm^2, and 14.75 mm^2, respectively. Similarly, damage estimated through the EP method, introduced in section II, is plotted in Figure 15 for transducer spacing $d = 400$ mm.

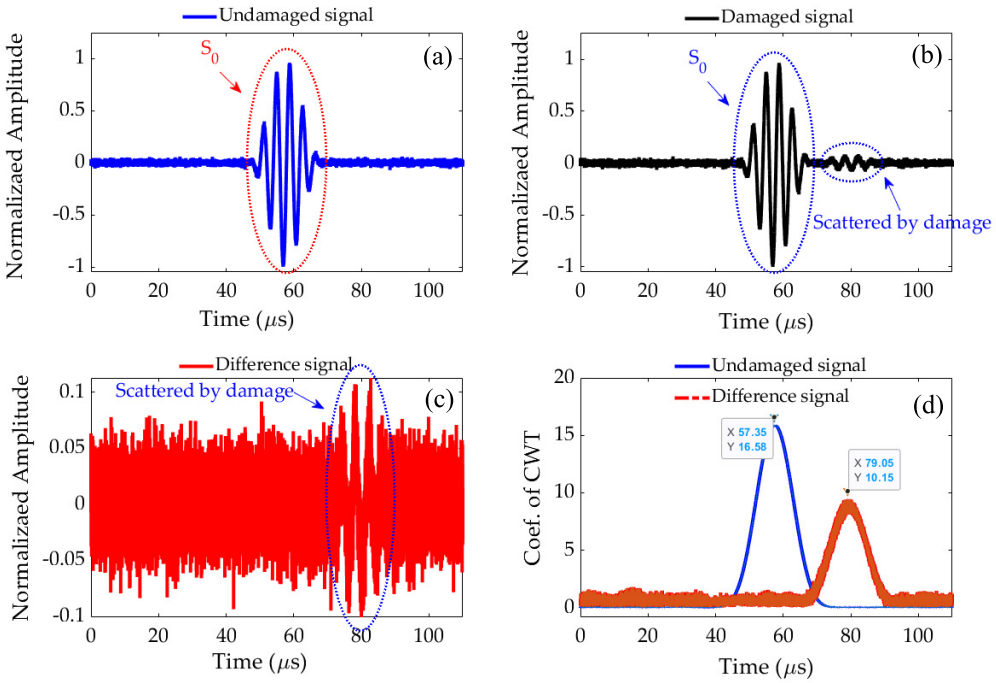

FIGURE 16. Undamaged signal at P2 with SNR = 20. (b) Damaged signal at P2 with SNR = 20. (c) Difference between undamaged and damaged signals with SNR = 20. (d) CWT of undamaged and difference signals with SNR = 20.

The estimated size of the damage was 40.08 mm^2, 36.65 mm^2, 36.58 mm^2, and 30.47 mm^2, respectively, for $d = 300, 400, 500, 600$ mm, and the absolute errors were 8.66 mm^2, 5.23 mm^2, 5.16 mm^2, and 0.95 mm^2, respectively. The results indicate that the EP method estimates the damage size with much higher accuracy than the CSC method. Furthermore, the error in damage size estimation also decreases as the size of the monitoring cell increases.

VIII. INFLUENCE OF NOISE ON DAMAGE ESTIMATION

In order to consider the noise tolerance of the proposed method for real-world problems, white noise signals in Gaussian distribution were artificially added to original undamaged and damaged signals presented in Figure 10. The signals are presented again in Figure 16 with high value of noise i.e., signal-to-noise ratio (SNR) = 20 dB. The noisy undamaged, damaged, difference and CWT signals are shown in Figure 16(a), (b), (c) and (d), respectively. The influence of noise on the signals can be observed by comparing the difference signals in Figure 10(c) and Figure 16(c). The delay times calculated from Figure 16(d) was $\boldsymbol{\Delta t_{02} = 21.7\ \mu s}$ while the same calculated from simulation signal was $\boldsymbol{\Delta t_{02} = 21.82\ \mu s}$. The noisy signals received in experiments are usually denoised first using different techniques. Therefore, the noisy undamaged and damaged signals in 16(a) and 16(b), respectively, were processed by 'Sym8' wavelet function in MATLAB to reduce the noise, and shown in Figure 17(a) and 17(b), respectively. The difference signal after denoising is presented in Figure 17(c), shows the reduction in noised when compared with noisy difference signal in Figure 16(c). The CWT of the denoised undamaged and difference signals are presented in Figure 17(d), and the delay time is calculated as $\boldsymbol{\Delta t_{02} = 21.73\ \mu s}$. Similarly, the delay times were calculated at all receivers for four values of SNR: 30, 40, 50 and 60. The damage location and size were then reevaluated for both noised and denoised cases, and compared with the simulation results.

For $d = 400$ mm, the comparison for location estimation is presented in Figure 18, size estimation for CSC method in Figure 19 and for EP method in Figure 20. The blue lines show the results for noisy signals, red lines show the denoised results whereas, the horizontal black dashed lines are the reference simulation results for the sake of comparison. Although, the accuracy of results fluctuates for noisy signals but the results are still in an acceptable range when compared with the simulation results. Furthermore, the accuracy becomes more stable and in accordance with the simulation results for the denoised cases.

IX. DISCUSSION OF RESULTS

The Lamb wave signals propagated radially outward in all directions and scattered by the damage in plate when a central PZT transducer was excited in the single-stage damage detection method. The single-stage method located the damage using centroid of intersections of elliptical path loci. The damage location could help to identify the damaged cell, and locate the triangular subcell containing the damage, which was required for improving the damage localization in the

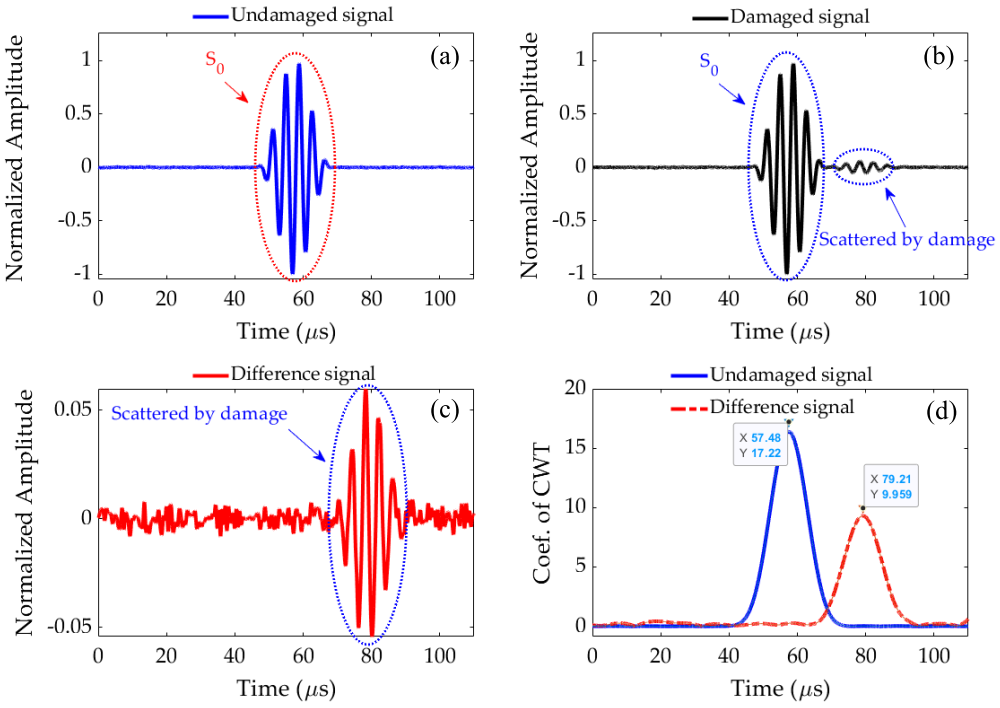

FIGURE 17. Denoised undamaged signal at P2 with SNR = 20. (b) Denoised damaged signal at P2 with SNR = 20. (c) Denoised difference between undamaged and damaged signals with SNR = 20. (d) Denoised CWT of undamaged and difference signals with SNR = 20.

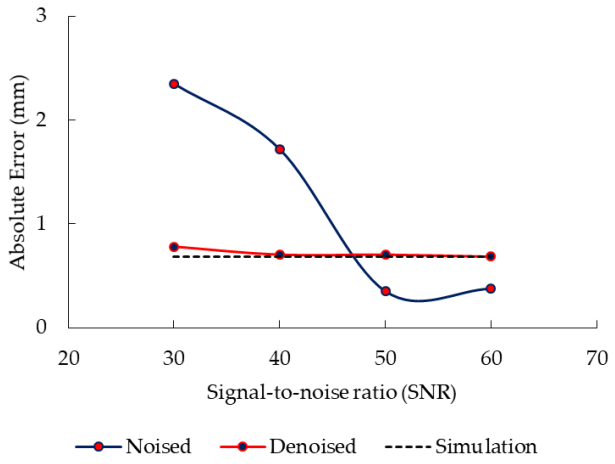

FIGURE 18. Comparison of damage location estimation for noised and denoised signals with the simulation results.

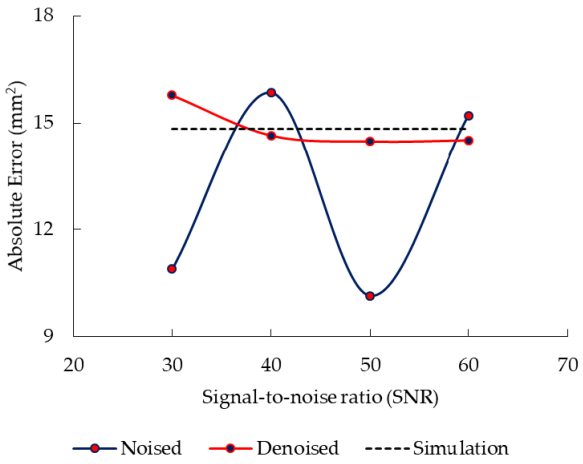

FIGURE 19. Comparison of damage size estimation for noised and denoised signals with the simulation results (CSC method).

two-stage detection. It is therefore proposed to separately excite the central transducer of each cell to find the damaged cells and subcells at this stage.

Using the same transducer arrangement, the damage localization could be improved in the two-stage detection by forming an additional corner ellipse around the triangular subcell, and using the two ellipses already formed in the single stage detection. The corner ellipse was produced by exciting a corner transducer and sensing at the other corner transducer separately inside the subcell. Therefore, the errors in damage localization could be reduced by estimating it with only three ellipses in the two-stage damage detection method.

The damage edge points were calculated by finding the shortest distance from the accurately estimated location of the damage. The damage size estimated through the CSC method defined the damage shape contour using the cubic spline curve passing through the damage edge points. The EP method estimated the damage shape as an ellipse whose parameters were defined using the same edge points. The EP method was found to be more accurate in estimating the size of the damage because it is more realistic estimation of the damage shape using only a few edge points. The size estimation using the CSC method could be improved by providing

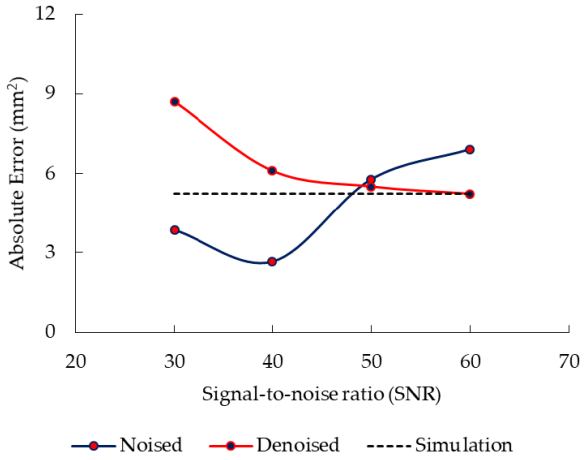

FIGURE 20. Comparison of damage size estimation for noised and denoised signals with the simulation results (EP method).

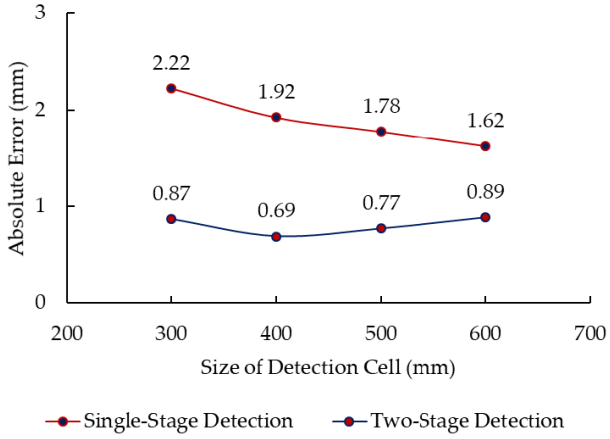

FIGURE 21. Effect of the size of detection cell on damage localization.

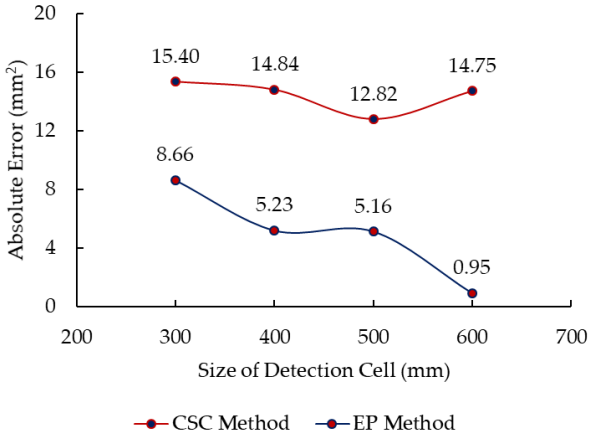

FIGURE 22. Comparison of damage size estimation using CSC and EP methods for different transducer spacing, d.

additional edge points at the expense of additional excitations and data recording. However, the motivation of this research is to develop a quantitative damage estimation method with minimum data recording during the on-line SHM for which the EP method is more suitable.

The absolute errors in evaluating the damage location, plotted in Figure 21 for all values of d, indicated an improvement in damage localization as the size of detection cell increased. It is due to the reason that the longer distance reduced the measurement error of delay time over the spacing $\Delta t/d$, as both sides of the nondimensional Equation (2) were divided by the distance d to calculate the damage location (x, y). The other reason is that the S_0 mode was better separated from the A_0 mode at longer distance d, and reduced the delay time errors. The recent studies have also provided the similar trends of reduction in error as the distance from the excitation increases for both metallic [38] and composite [48] plates.

The absolute errors for damage size estimation, using both the CSC and EP methods, are plotted in Figure 22 for all values of d. The results indicate that the EP method estimates the damage size with much higher accuracy than the CSC method. The results improved reasonably well when the size was estimated using bigger path loci, therefore, the damage extent can be better detected in the bigger cells formed by the network of transducers.

It can be concluded from the trends shown in Figure 21 and Figure 22 that the bigger ellipses formed inside the bigger detection cells provided more accurate damage detection. Therefore, the single-stage provided a fast detection with only one excitation whereas, two-stage improved the detection results with an additional large ellipse using an extra excitation. This is because the single-stage obtained the elliptical path loci with transducer spacing $\frac{\sqrt{2}}{2}\boldsymbol{d}$, the additional ellipse in the second-stage was obtained by the corner transducers with larger spacing d. The longer distance reduced the error in calculating the delay time by Equation (2).

Generally, a higher error is expected in the bigger cells due to the dispersive behavior of the Lamb wave signals, which causes inaccuracies in measuring the delay times. However, the accuracy of the proposed damage detection method improves as the size of detection cell increases because the CWT is a better time-frequency representative. The CWT could depress the dispersive characteristics effectively, had a better SNR, and could accurately extract the time-frequency feature from the noisy signals.

X. CONCLUSION

The transverse damage in composite laminates is generally induced during the manufacturing and in-service processes. The non-ignorable size of transverse damage in composite laminates has an adverse effect on ellipse-based damage detection methods. The PZT transducers arranged in the form of network of cells helps in practice to estimate the damage locally inside each of the cells. The centroid of intersections of path loci provides a highly accurate damage localization in two stages. The single-stage detection can be conducted simultaneously in each cell of a large PZT transducer network for damage localization, and further to identify the cells and subcells containing the damage. In order to further improve the damage localization, the second stage can be conducted

only inside the damaged subcell. The accurately estimated damage location then helps to determine the edge points which are essential for damage size estimation. Two novel methods, CSC and EP, for quantitative damage size estimation are presented, and their performances are compared. The amount of data collected in the proposed method is small as compared to the existing ellipse-based methods. It is due to a small number of PZT transducers used to form the detection cells. Only two excitations in total are required: one excitation each in the first and second stage. The data collected in the single-stage for damage localization is reused in the second stage for improved localization, and then also for the quantitative damage sizing. Therefore, both the computational time and evaluation cost can be saved during the NDT/SHM process using the proposed method, that is why the method is also suitable for on-line monitoring. Furthermore, the implementation of the proposed method is relatively simple and straightforward for efficient damage detection in composite laminates frequently used in civil, automobile, aerospace, marine, and wind turbine industries etc. However, the focus of this research was to initially develop the method and test it for the simplified cases e.g., the quasi-isotropic composite laminates were used, and the elliptical damage was made as a through-hole in simulations which may be different than the delamination in composite laminates.

REFERENCES

[1] G. F. Gomes, Y. A. D. Mendéz, P. da Silva Lopes Alexandrino, S. S. da Cunha, Jr., and A. C. Ancelotti, Jr., "The use of intelligent computational tools for damage detection and identification with an emphasis on composites—A review," *Compos. Struct.*, vol. 196, pp. 44–54, Jul. 2018.

[2] Z. Su and L. Ye, *Identification of Damage Using Lamb Waves*. London, U.K.: Springer-Verlag, 2009.

[3] K. Zheng, Z. Li, Z. Ma, J. Chen, J. Zhou, and X. Su, "Damage detection method based on Lamb waves for stiffened composite panels," *Compos. Struct.*, vol. 225, Oct. 2019, Art. no. 111137.

[4] G. Yan, "A Bayesian approach for damage localization in plate-like structures using Lamb waves," *Smart Mater. Struct.*, vol. 22, no. 3, 2013, Art. no. 035012.

[5] M. Niethammer, L. J. Jacobs, J. Qu, and J. Jarzynski, "Time-frequency representations of Lamb waves," *J. Acoust. Soc. Amer.*, vol. 109, no. 5, p. 1841, 2006.

[6] L. De Marchi, A. Marzani, S. Caporale, and N. Speciale, "Ultrasonic guided-waves characterization with warped frequency transforms," *IEEE Trans. Ultrason., Ferroelectr., Freq. Control*, vol. 56, no. 10, pp. 2232–2240, Oct. 2009.

[7] A. Raghavan and C. E. S. Cesnik, "Guided-wave signal processing using chirplet matching pursuits and mode correlation for structural health monitoring," *Smart Mater. Struct.*, vol. 16, no. 2, pp. 355–366, 2007.

[8] F. Gao, J. Hua, L. Zeng, and J. Lin, "Amplitude modified sparse imaging for damage detection in quasi-isotropic composite laminates using non-contact laser induced Lamb waves," *Ultrasonics*, vol. 93, pp. 122–129, Mar. 2019.

[9] J. S. Hall and J. E. Michaels, "Minimum variance ultrasonic imaging applied to an *in situ* sparse guided wave array," *IEEE Trans. Ultrason., Ferroelectr., Freq. Control*, vol. 57, no. 10, pp. 2311–2323, Oct. 2010.

[10] D. Wang, W. Zhang, X. Wang, and B. Sun, "Lamb-wave-based tomographic imaging techniques for hole-edge corrosion monitoring in plate structures," *Materials*, vol. 9, no. 11, p. 916, 2016.

[11] J. Qiu, F. Li, S. Abbas, and Y. Zhu, "A baseline-free damage detection approach based on distance compensation of guided waves," *J. Low Freq. Noise, Vib. Active Control*, vol. 38, nos. 3–4, pp. 1132–1148, 2018.

[12] C. Zhou, Z. Su, and L. Cheng, "Probability-based diagnostic imaging using hybrid features extracted from ultrasonic Lamb wave signals," *Smart Mater. Struct.*, vol. 20, no. 12, 2011, Art. no. 125005.

[13] J. He, D. C. Rocha, P. E. Leser, P. Sava, and W. P. Leser, "Least-squares reverse time migration (LSRTM) for damage imaging using Lamb waves," *Smart Mater. Struct.*, vol. 28, no. 6, 2019, Art. no. 065010.

[14] R. Gorgin, Z. Wu, D. Gao, and Y. Wang, "Damage size characterization algorithm for active structural health monitoring using the A_0 mode of Lamb waves," *Smart Mater. Struct.*, vol. 23, no. 3, 2014, Art. no. 035015.

[15] J.-B. Ihn and F.-K. Chang, "Pitch-catch active sensing methods in structural health monitoring for aircraft structures," *Struct. Health Monit.*, vol. 7, no. 1, pp. 5–15, 2008.

[16] G. Lu, Y. Li, M. Zhou, Q. Feng, and G. Song, "Detecting damage size and shape in a plate structure using PZT transducer array," *J. Aerosp. Eng.*, vol. 31, no. 5, 2018, Art. no. 04018075.

[17] N. Hu, Y. Cai, G. Zhu, C. Tsuji, Y. Liu, and Y. Cao, "Characterization of damage size in metallic plates using Lamb waves," *Struct. Health Monit.*, vol. 11, no. 2, pp. 125–137, 2012.

[18] F. Gao, L. Zeng, J. Lin, and Y. Shao, "Damage assessment in composite laminates via broadband Lamb wave," *Ultrasonics*, vol. 86, pp. 49–58, May 2018.

[19] B. Yang, F.-Z. Xuan, P. Jin, C. Hu, B. Xiao, D. Li, Y. Xiang, and H. Lei, "Damage localization in composite laminates by building in PZT wafer transducers: A comparative study with surface-bonded PZT strategy," *Adv. Eng. Mater.*, vol. 21, no. 3, Mar. 2019, Art. no. 1801040.

[20] P. Kudela, M. Radzienski, W. Ostachowicz, and Z. Yang, "Structural health monitoring system based on a concept of Lamb wave focusing by the piezoelectric array," *Mech. Syst. Signal Process.*, vol. 108, pp. 21–32, Aug. 2018.

[21] C.-B. Xu, Z.-B. Yang, X.-F. Chen, S.-H. Tian, and Y. Xie, "A guided wave dispersion compensation method based on compressed sensing," *Mech. Syst. Signal Process.*, vol. 103, pp. 89–104, Mar. 2018.

[22] D. Dinh-Cong, T. Vo-Duy, N. Nguyen-Minh, V. Ho-Huu, and T. Nguyen-Thoi, "A two-stage assessment method using damage locating vector method and differential evolution algorithm for damage identification of cross-ply laminated composite beams," *Adv. Struct. Eng.*, vol. 20, no. 12, pp. 1807–1827, 2017.

[23] D. Dinh-Cong, H. Dang-Trung, and T. Nguyen-Thoi, "An efficient approach for optimal sensor placement and damage identification in laminated composite structures," *Adv. Eng. Softw.*, vol. 119, pp. 48–59, May 2018.

[24] G. Liu, Y. Xiao, H. Zhang, and G. Ren, "Elliptical ring distribution probability-based damage imaging method for complex aircraft structures," *J. Vibroeng.*, vol. 19, no. 7, pp. 4936–4952, 2017.

[25] B. Feng, D. J. Pasadas, A. L. Ribeiro, and H. G. Ramos, "Locating defects in anisotropic CFRP plates using ToF-based probability matrix and neural networks," *IEEE Trans. Instrum. Meas.*, vol. 68, no. 5, pp. 1252–1260, May 2019.

[26] Z. Wang, Z. Xiao, Y. Li, and Y. Jiang, "An omnidirectional near-field comprehensive damage detection method for composite structures," *Appl. Sci.*, vol. 9, no. 3, p. 567, 2019.

[27] W. Gao, L. Huo, H. Li, and G. Song, "An embedded tubular PZT transducer based damage imaging method for two-dimensional concrete structures," *IEEE Access*, vol. 6, pp. 30100–30109, 2018.

[28] B. Li, Y. Liu, K. Gong, and Z. Li, "Damage localization in composite laminates based on a quantitative expression of anisotropic wavefront," *Smart Mater. Struct.*, vol. 22, no. 6, 2013, Art. no. 065005.

[29] A. Bagheri, K. Li, and P. Rizzo, "Reference-free damage detection by means of wavelet transform and empirical mode decomposition applied to Lamb waves," *J. Intell. Mater. Syst. Struct.*, vol. 24, no. 2, pp. 194–208, Jan. 2013.

[30] I. Amenabar, A. Mendikute, A. López-Arraiza, M. Lizaranzu, and J. Aurrekoetxea, "Comparison and analysis of non-destructive testing techniques suitable for delamination inspection in wind turbine blades," *Compos. B, Eng.*, vol. 42, no. 5, pp. 1298–1305, 2011.

[31] R.-F. Zheng, T.-H. Wu, and X.-Y. Li, "Elliptic crack in transversely isotropic magneto-electro-elasticity under shear loading," *Int. J. Eng. Sci.*, vol. 134, pp. 47–65, Jan. 2019.

[32] T. J. Vaughan and C. T. McCarthy, "Micromechanical modelling of the transverse damage behaviour in fibre reinforced composites," *Compos. Sci. Technol.*, vol. 71, no. 3, pp. 388–396, 2011.

[33] M. Gentz, D. Armentrout, P. Rupnowski, L. Kumosa, E. Shin, J. K. Sutter, and M. Kumosa, "In-plane shear testing of medium and high modulus woven graphite fiber reinforced/polyimide composites," *Compos. Sci. Technol.*, vol. 64, no. 2, pp. 203–220, 2004.

[34] F. Xu, I. A. Jones, and S. Li, "A continuum damage model for transverse cracking in UD composites of linear viscoelastic behaviour," *Compos. Struct.*, vol. 225, Oct. 2019, Art. no. 110812.
[35] B. Li, L. Ye, Z. Li, Z. Ma, and H. Kalhori, "Quantitative identification of delamination at different interfaces using guided wave signals in composite laminates," *J. Reinforced Plastics Compos.*, vol. 34, no. 18, pp. 1506–1525, 2015.
[36] H. Li, Z. Wang, J. Y.-L. Forrest, and W. Jiang, "Low-velocity impact localization on composites under sensor damage by interpolation reference database and fuzzy evidence theory," *IEEE Access*, vol. 6, pp. 31157–31168, 2018.
[37] J. Chen, Z. Li, and K. Gong, "Nondestructive testing method based on Lamb waves for localization and extent of damage," *Acta Mech. Solida Sinica*, vol. 30, no. 1, pp. 65–74, 2017.
[38] M. S. Hameed, Z. Li, J. Chen, and J. Qi, "Lamb-wave-based multistage damage detection method using an active PZT sensor network for large structures," *Sensors*, vol. 19, no. 9, p. 2010, Apr. 2019.
[39] E. T. Y. Lee, "Choosing nodes in parametric curve interpolation," *Comput.-Aided Des.*, vol. 21, no. 6, pp. 363–370, 1989.
[40] H. Kaczmarek, "Lamb wave interaction with impact-induced damage in aircraft composite: Use of the A_0 mode excited by air-coupled transducer," *J. Compos. Mater.*, vol. 37, no. 3, pp. 217–232, 2003.
[41] Z. Ma, J. Chen, B. Li, Z. Li, and X. Su, "Dispersion analysis of Lamb waves in composite laminates based on reverberation-ray matrix method," *Compos. Struct.*, vol. 136, pp. 419–429, Feb. 2016.
[42] D. V. Achillopoulou and A. Pau, "Characterization of defects in plates using shear and Lamb waves," *Procedia Eng.*, vol. 199, pp. 2001–2007, Sep. 2017.
[43] L. Wang and F. G. Yuan, "Group velocity and characteristic wave curves of Lamb waves in composites: Modeling and experiments," *Compos. Sci. Technol.*, vol. 67, pp. 1370–1384, Jun. 2007.
[44] B. Hu, N. Hu, L. Li, W. Li, S. Tang, Y. Li, X. Peng, A. Homma, Y. Liu, L. Wu, and H. Ning, "Tomographic reconstruction of damage images in hollow cylinders using Lamb waves," *Ultrasonics*, vol. 54, no. 7, pp. 2015–2023, 2014.
[45] X. Liu, L. Bo, Y. Liu, Y. Zhao, J. Zhang, N. Hu, S. Fu, and M. Deng, "Detection of micro-cracks using nonlinear Lamb waves based on the Duffing–Holmes system," *J. Sound Vib.*, vol. 405, pp. 175–186, Sep. 2017.
[46] X. Wang, G. Foliente, Z. Su, and L. Ye, "Multilevel decision fusion in a distributed active sensor network for structural damage detection," *Struct. Health Monit.*, vol. 5, no. 1, pp. 45–58, Mar. 2006.
[47] Y. Liu, Z. Li, and W. Zhang, "Crack detection of fibre reinforced composite beams based on continuous wavelet transform," *Nondestruct. Test. Eval.*, vol. 25, no. 1, pp. 25–44, 2010.
[48] L. Maio, F. Ricci, V. Memmolo, E. Monaco, and N. D. Boffa, "Application of laser Doppler vibrometry for ultrasonic velocity assessment in a composite panel with defect," *Compos. Struct.*, vol. 184, pp. 1030–1039, Jan. 2018.

M. SAQIB HAMEED received the B.S. degree in aerospace engineering from the Institute of Space Technology, Islamabad, in 2008, the M.S. degree (Hons.) in mechanical design engineering from HITEC University, Pakistan, and the M.S. degree in computational civil engineering from Swansea University, U.K. He is currently pursuing the Ph.D. degree with Peking University (PKU), Beijing. He has over seven years' experience of teaching mechanical engineering courses at HITEC University and COMSATS University, Islamabad (CUI). He is also designated as an Assistant Professor in the faculty of mechanical engineering with CUI. He has authored/coauthored 17 journal and conference papers. His research interests include the development of nondestructive testing methods for aerospace and turbine structures. He is also working on guided wave-based and vibration-based structural health monitoring methods for composite laminates. He was a recipient of Chinese government scholarship, Ph.D. class-III scholarship of PKU, European commission's Erasmus Mundus fellowship, and HITEC University's scholarship for faculty development. He was also awarded with the Outstanding Research Award by PKU, in 2019, and the Research Productivity Award by CUI, in 2013 and 2015.

ZHENG LI received the B.S., M.S., and Ph.D. degrees from Peking University, Beijing, China. She is currently a Full Professor with the Department of Mechanics and Engineering Science, Peking University. She has published over 100 research articles in the prestigious international journals. She has presented her work at a number of renown conferences around the world. Her research interests include nondestructive testing and structural health monitoring methods, experimental mechanics in dynamic fracture, stress wave propagation, and mechanical behavior of advanced materials. She is a member of Chinese Experimental Mechanics Society. She is the editorial board member of professional journals, such as *Mechanics in Engineering*, *Chinese Quarterly of Mechanics*, and the *Journal of Experimental Mechanics*.